

**Supplemental Information**

**Distal Alternative Last Exons**

**Localize mRNAs to Neural Projections**

**J. Matthew Taliaferro, Marina Vidaki, Ruan Oliveira, Sara Olson, Lijun Zhan, Tanvi Saxena, Eric T. Wang, Brenton R. Graveley, Frank B. Gertler, Maurice S. Swanson, and Christopher B. Burge**

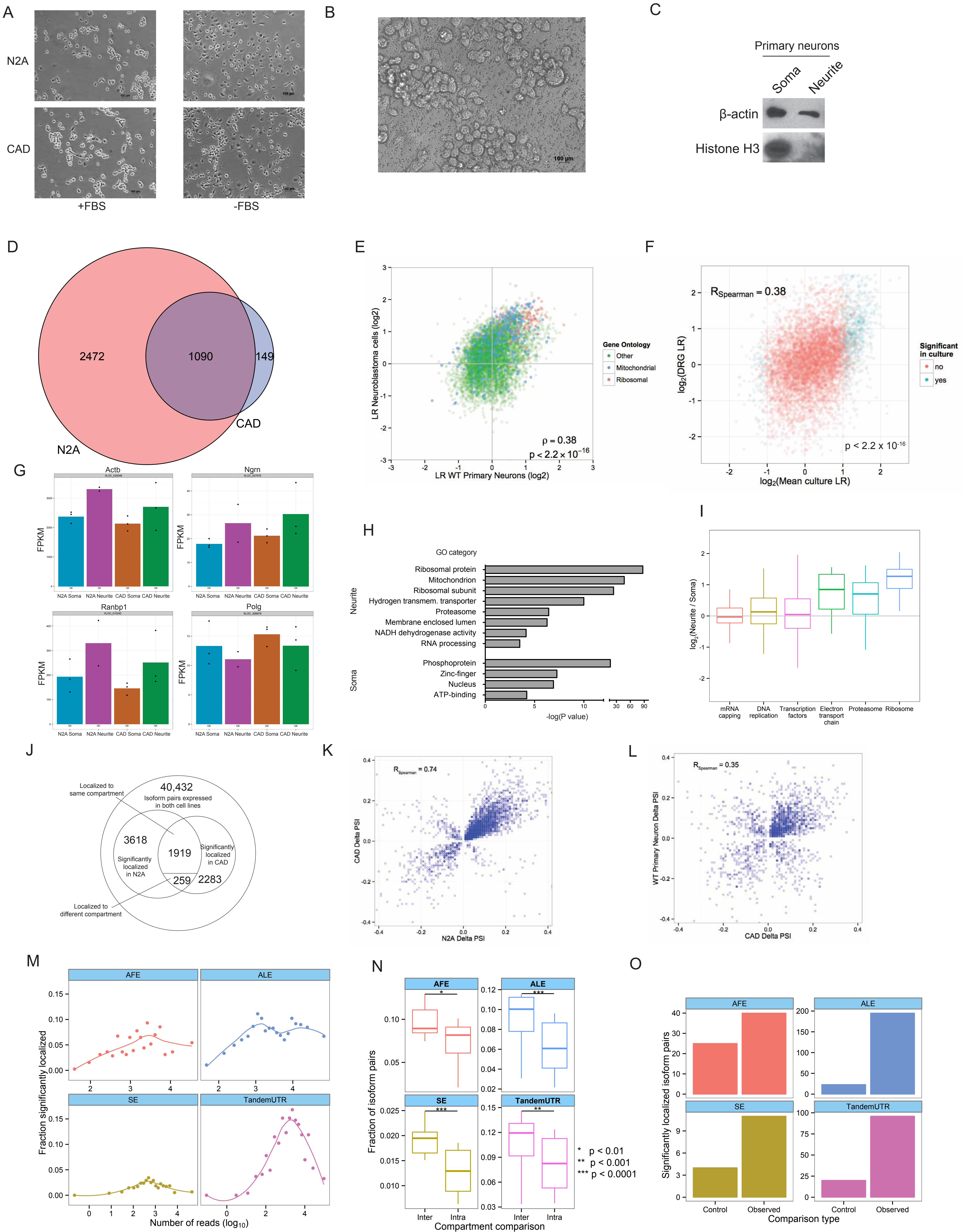
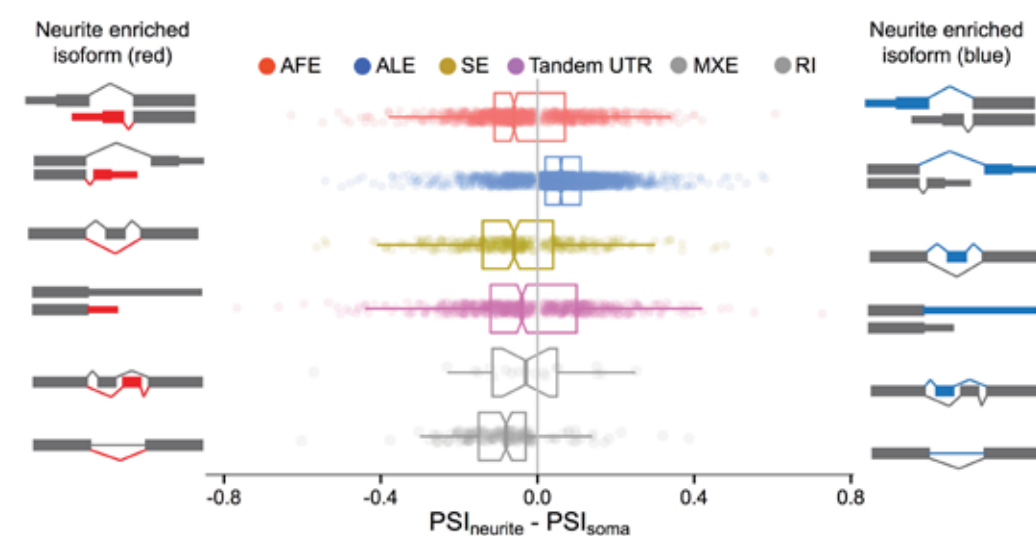
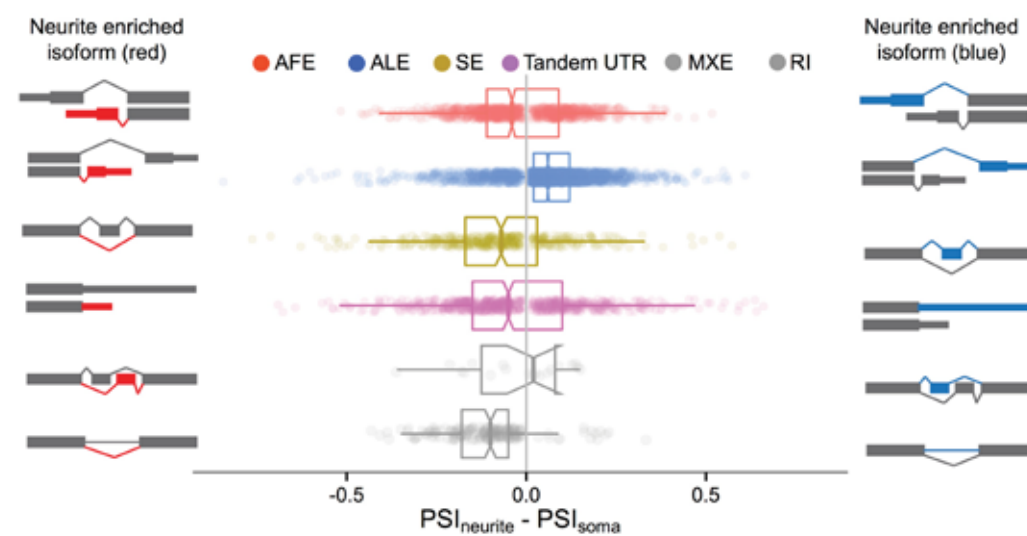


Figure S1

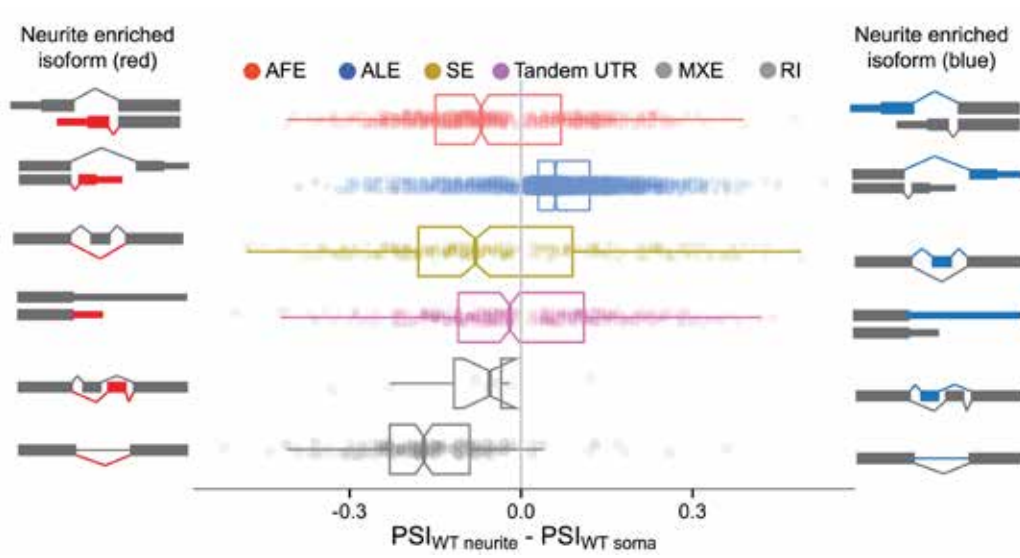
A



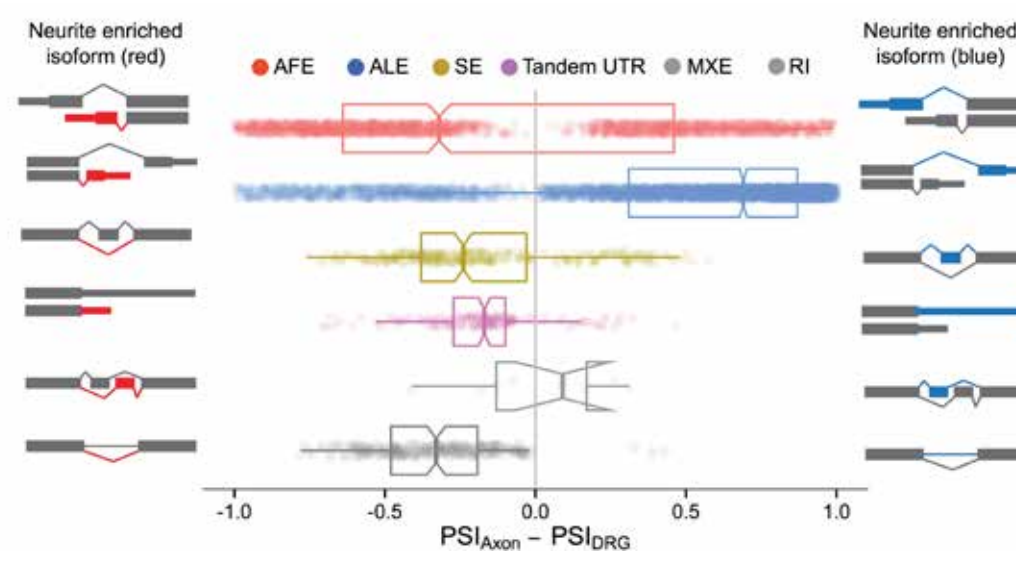
B



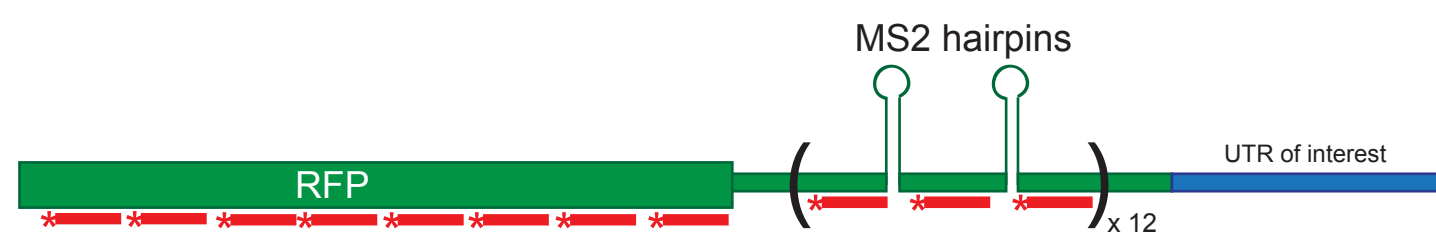
C



D

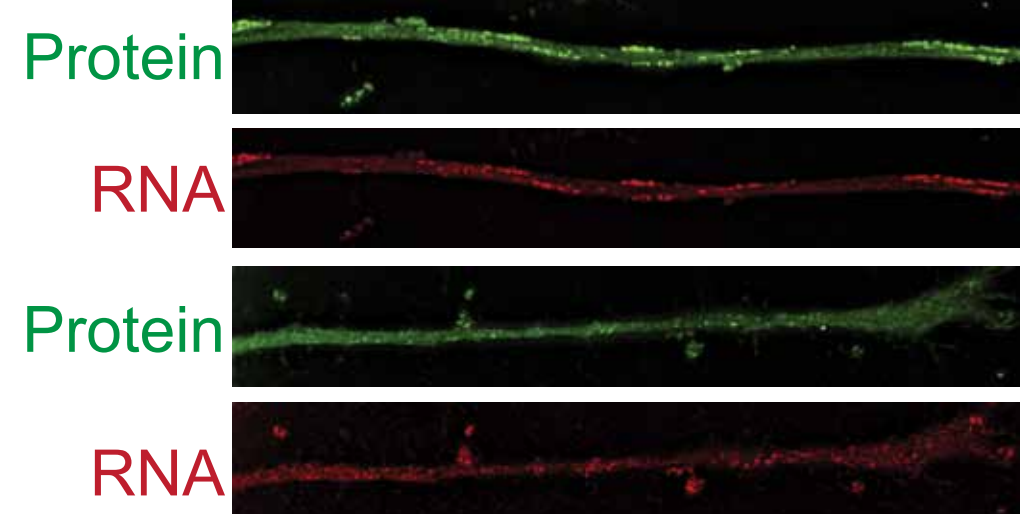


E

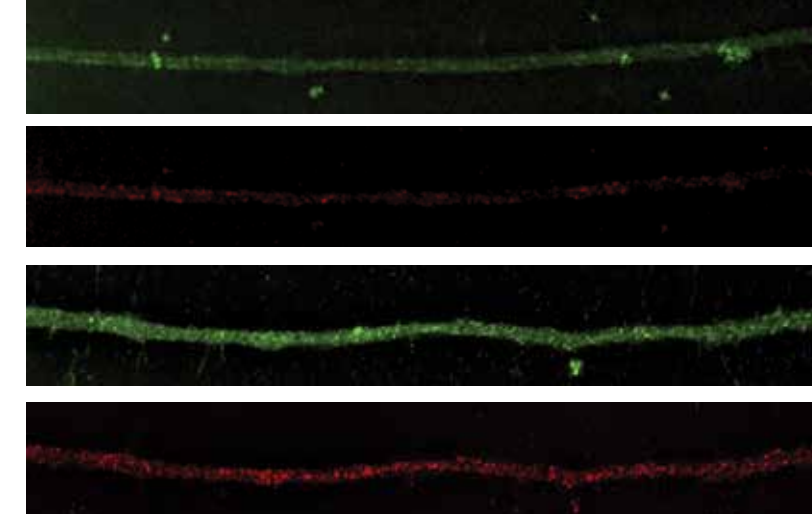


F

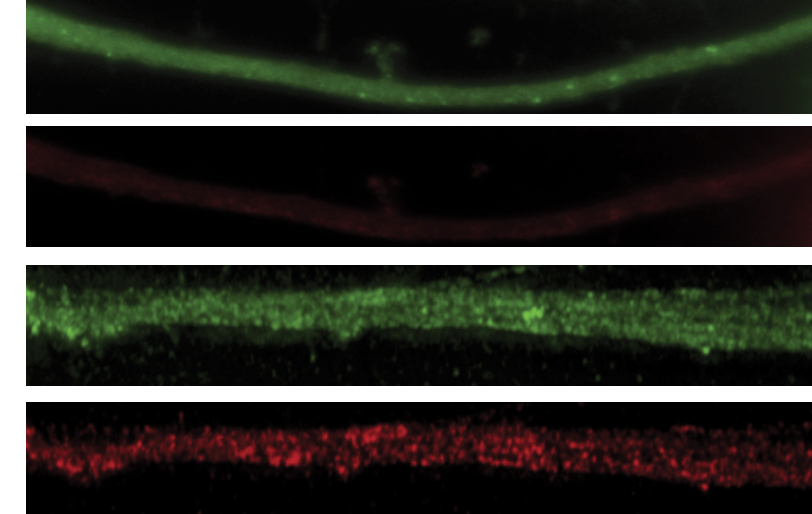
Phf12



Rdh5



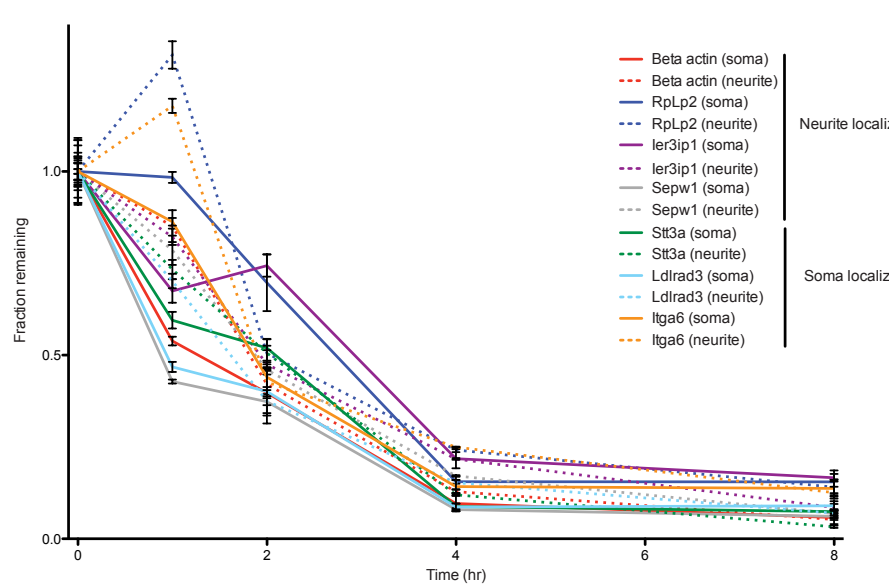
Cul9



Proximal UTR

Distal UTR

G



H

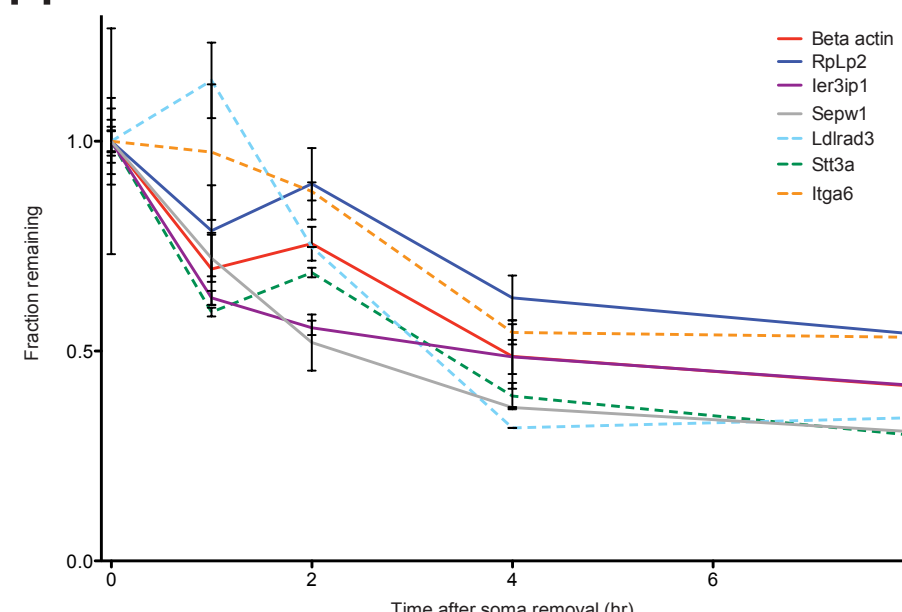


Figure S2

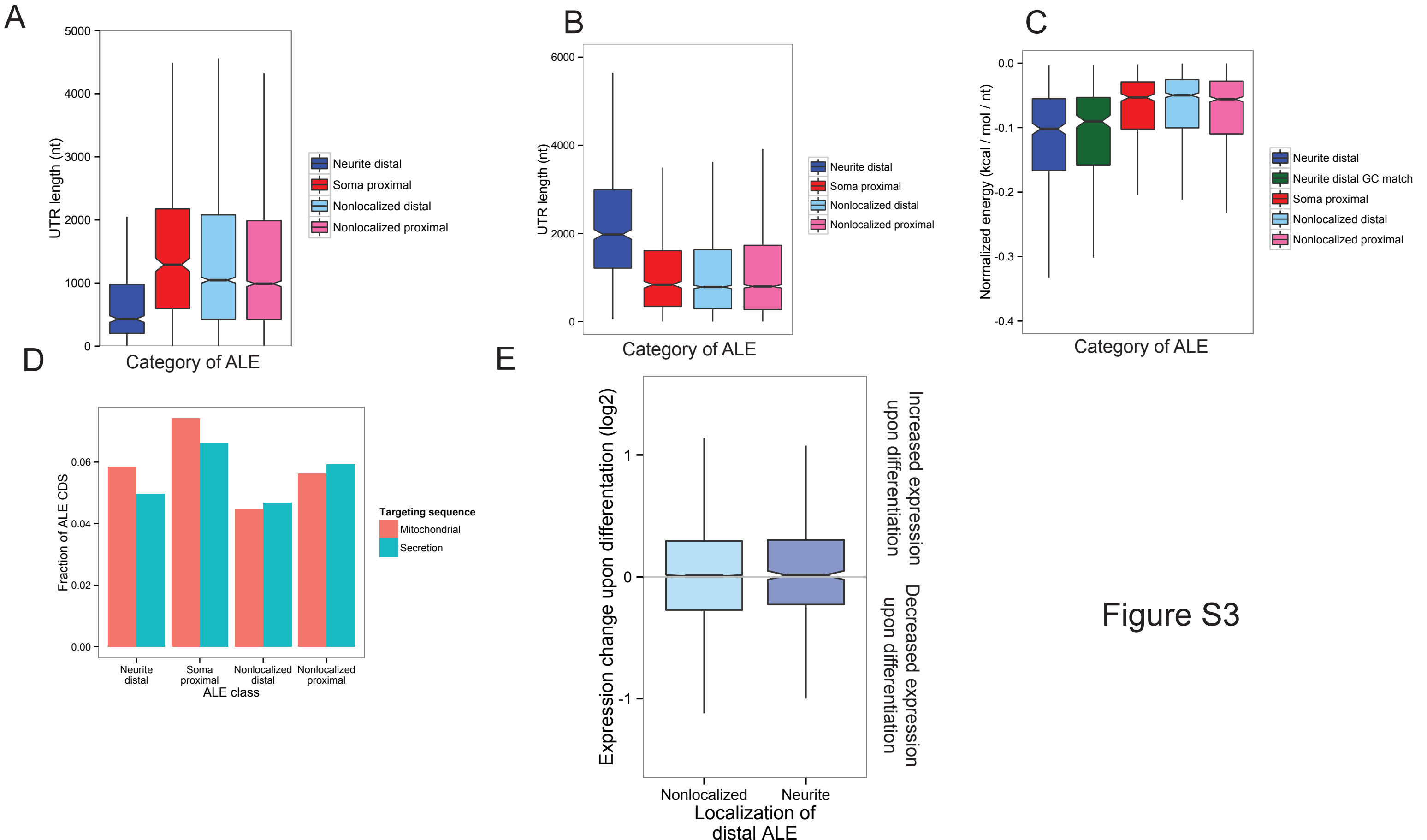
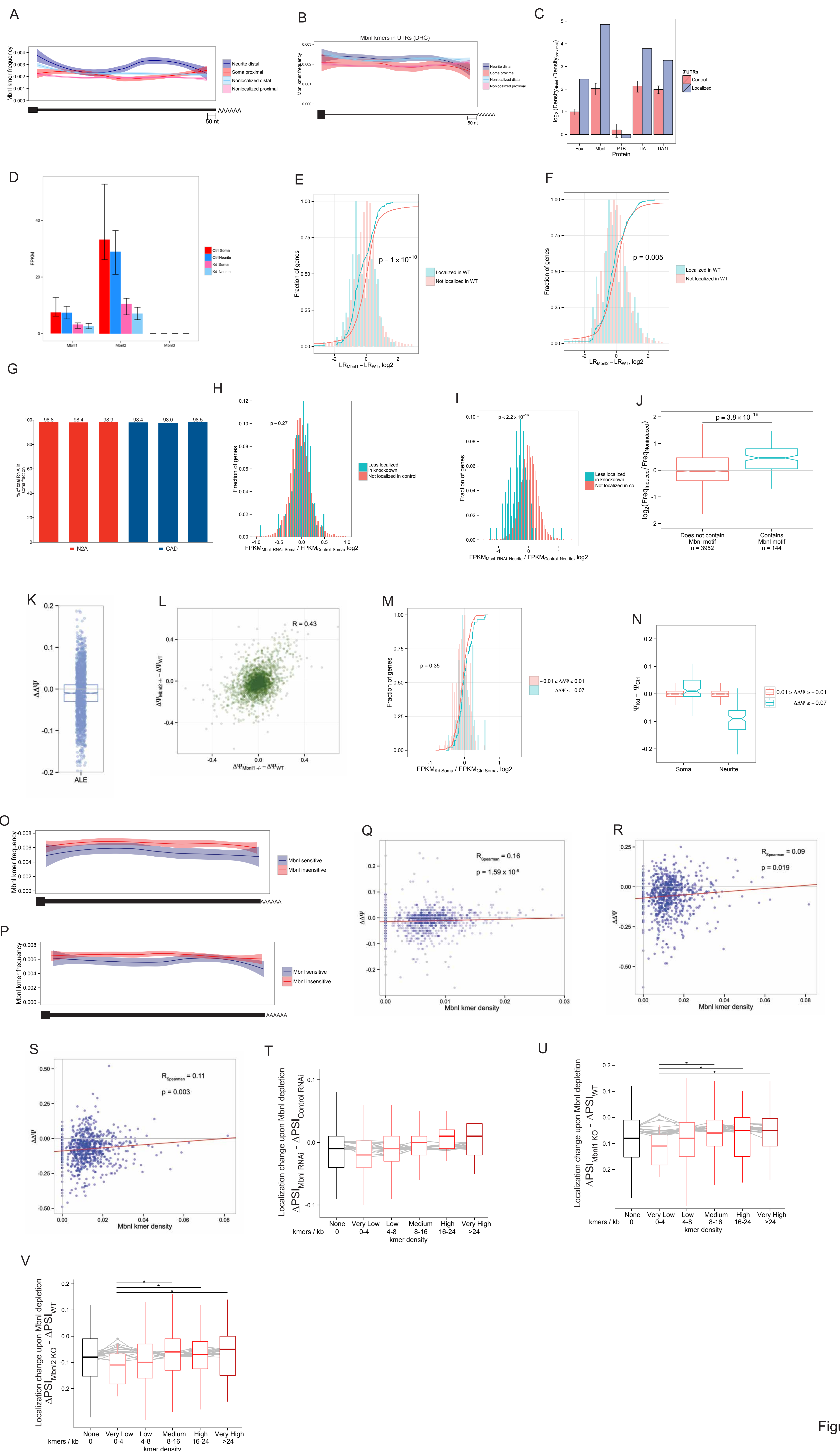


Figure S3



## Legends to Supplementary Figures

**Figure S1. Related to Figure 1. Gene expression and alternative splicing analyses of subcellular transcriptomes.** A) N2A and CAD cells before and after serum withdrawal. Scale bars are 100 micrometers. B) N2A cells on porous membrane used for subcellular fractionation. Pore sizes are much smaller than cell diameters. C) Soma and neurite lysates from primary cortical neurons were immunoblotted for the presence of beta-actin, a marker of both soma and neurite fractions, and histone H3, a marker of soma fractions. D) Overlap of genes called by Cuffdiff as significantly enriched in either the soma or neurite fraction in N2A and CAD cells. E) Comparison of localization ratios from cell culture experiments and cortical neurons from E18.5 mice. Culture localization ratio values are the mean of localization ratios in N2A and CAD cells. F) Comparison of localization ratios from cell culture experiments and subcellular RNAseq data produced in dorsal root ganglia (Minis et al., 2013). Culture localization ratio values are the mean of localization ratios in N2A and CAD cells. G) FPKM values from N2A and CAD subcellular fractions for three genes known to localize to neuronal projections, beta-actin, neurogranin, and Ranbp1. *Polg* is a subunit of the mitochondrial DNA polymerase. (Bassell et al., 1998; Gao et al., 2008; Yudin et al., 2008) H) Gene ontology categories of genes enriched in the neurite (top) or soma (bottom) fractions of N2A and CAD cells. I) Distribution of LRs in the two cell lines for genes with the indicated gene ontology annotations. J) Number of alternative splicing events significantly differentially enriched between cell body and neurite fractions in N2A and CAD cells. In total 40,432 isoform pairs were interrogated. K) ALE  $\Delta\Psi$  values for events significantly enriched in both cell lines, separated by event type.  $\Delta\Psi$  is defined as the PSI for an event in the neurite minus the PSI in the soma. L) Comparison of ALE delta PSI values obtained from the two cell lines and primary cortical neurons from WT mice. M) The fraction of the expressed isoform pairs that were significantly differentially enriched between soma and neurite fractions expressed as a function of the read coverage for that event. N) Control for difference in power between event types with which differentially enriched events are detected. The fraction of total events that

appeared significantly enriched between all possible comparisons of replicates was calculated and is represented on the y-axis. If the comparison was between two soma or two neurite samples, it was recorded as “intracompartamental” while comparisons across compartments were “intercompartmental”. The “intracompartamental” comparisons are therefore analogous to control comparisons where RNA from the same cellular compartment is compared. Comparing the fraction of events identified as enriched between intercompartmental and intracompartamental comparisons, then, controls for the different rates with which each event type is detected by RNA-seq. O) Estimation of FDR in calling differentially localized isoforms. Isoform pairs were called as significant if they met filters (Bayes factor of at least 10,  $\Delta\Psi \geq 0.1$ ) in at least 2 of 3 replicates in both N2A and CAD cells and also had the same sign of delta PSI in each cell line. “Control” comparisons were made between samples from the same compartment of the same cell line while “actual” comparisons were made between samples from different compartments of the same cell line.

**Figure S2. Related to Figure 2. Alternative splice isoform localization in neuronal samples and the effects of RNA decay on subcellular gene expression measurements.** A) Distribution of delta PSI values for significantly enriched events from fractionation of CAD cells, including RI and MXE events. B) Distribution of delta PSI values for significantly enriched events from fractionation of N2A cells. C) Distribution of delta PSI values for significantly enriched events from fractionation of primary cortical neurons. D) Distribution of PSI values for significantly enriched events from fractionation of peripheral axons from dorsal root ganglia. E) Schematic of RNA FISH reporter construct. The construct consists of the open reading frame of RFP (pseudo-colored green in images), followed by 24 MS2 hairpins, followed by the UTR of interest. FISH probes (pseudo-colored red in images) are designed against the RFP ORF and regions of the MS2 hairpin module not excluded by hairpin formation. F) Images from Figures 2A and 2B, with the protein and RNA fluorescent signals separated. G) RNA decay analysis of 4 projection-enriched and 3 cell body-enriched genes using actinomycin D and qRT-PCR. RNA was collected from cell body (solid line)

or neurite (dotted line) fractions of N2A cells at the indicated time points after treatment with actinomycin D. H) Same as (G), except that the arrival of new RNA is neurites was halted by the removal of cell bodies rather than treatment with actinomycin D. RNA was collected at the indicated time points after removal of cell bodies.

**Figure S3. Related to Figure 3. Properties of localized and nonlocalized ALEs in primary cortical neurons and DRG.** A) Distribution of UTR lengths for localized and nonlocalized UTRs derived from subcellular fractionation of WT primary cortical neurons. B) Distribution of UTR lengths for localized and nonlocalized UTRs derived from subcellular fractionation of dorsal root ganglia (Minis et al., 2013). C) Distribution of secondary structure folding energies for indicate UTRs identified in N2A and CAD cells calculated by RNALfold. RNALfold searches for locally stable structures up to a given size, in this case 150 nt. For each RNA, the reported folding energy was the stablest local structure found in that RNA, normalized by the length of the RNA. In the GC match class, the GC content of the ‘neurite distal’ class was subsampled to match that of the ‘soma proximal’ class. D) The coding portions of alternative last exons from the indicated classes were interrogated using TargetP (Emanuelsson et al., 2000) to search for signal polypeptide sequences that are associated with targeting the protein to the mitochondria or secretory pathways. The fraction of ALE events in each class with predicted signal sequences is shown. E) Change in expression upon differentiation of CAD cells of genes that do not (left) or do (right) contain alternative last exons events associated with localization.

**Figure S4. Related to Figure 4. Effects of Mbnl depletion on RNA localization.** A) Metagene analysis of Mbnl sequence sites across UTRs of the indicated classes. UTRs were classified based on the  $\Delta\Psi$  values of their ALEs in cortical neurons. The last 50 nt of each UTR was removed to discount the presence of polyadenylation sequences. B) Similar to (A), except that UTRs were classified based on the  $\Delta\Psi$  values of their ALEs in DRG. C) Similar to Figure 4C, CLIP-seq clusters identified in mouse brain were intersected with localized and control UTRs identified in mouse dorsal root ganglia

(Minis et al., 2013). Control UTRs consist of 3 sets of randomly selected UTRs from ALE events not associated with localization. D) FPKM values for muscleblind proteins in N2A and CAD soma and neurite fractions followed treatment with control and Mbnl siRNAs. E-F) Changes in cortical neuron localization ratios in *Mbnl1* knockouts (E) and *Mbnl2* knockouts (F) relative to WT mice. Localized genes are defined as those which were called by Cuffdiff as differentially enriched between soma and neurite fractions in WT mice. G) Following cell fractionation and RNA isolation, RNA quantities in both fractions were measured. Bars indicate the fraction of combined soma and neurite RNA that was recovered from the soma fraction. H) Change in CAD somal expression for localized and non-localized genes. I) Change in CAD neurite expression for localized and non-localized genes. J) PSI values for ALE events were calculated before and after differentiation of human neural precursor cells to neurons (Sauvageau et al., 2013, Fig. 3E). Distal ALEs were defined as induced to inclusion if their change in PSI value (Differentiation Day18 PSI – Differentiation Day0 PSI) was greater than or equal to 0.10. Conversely, Distal ALEs were defined as non-induced if their change in PSI value was between –0.02 and 0.02. In total, 237 distal ALEs were induced and 487 were noninduced. The frequency of all 6mers in the UTRs of each set of ALEs was then calculated, normalized to the length of each UTR, and the enrichment for a 6mer defined as its frequency in the induced ALEs divided by its frequency in the noninduced ALEs. If a 6mer contained UGCU, UGCC, or CGCU, it was defined as containing a Mbnl site and went into the bin on the right. If not, it went into the bin on the left. (K)  $\Delta\Delta\Psi$  PSI values for alternative splicing events in CAD cells. Delta PSI values are calculated as PSI in the neurite minus PSI in the soma.  $\Delta\Delta\Psi$  values are calculated as  $\Delta\Psi$  in the Mbnl knockdown sample minus  $\Delta\Psi$  in the control sample. L) Comparison of  $\Delta\Delta\Psi$  values in cortical neurons from *Mbnl1* and *Mbnl2* knockout mice for ALE events. M) Change in expression for genes containing ALE events whose  $\Delta\Psi$  values were sensitive (blue) or insensitive (pink) to muscleblind knockdown in CAD cells. Sensitivity was defined as having a  $\Delta\Delta\Psi$  value at least 1 SD below the mean. Insensitive ALEs were defined as having delta delta PSI values between –0.01 and 0.01. N)  $\Delta\Psi$  values (Mbnl knockdown minus control) in each compartment for events with the indicated

delta delta PSI values. Here, a positive  $\Delta\Psi$  indicates an increase in the expression of the distal ALE in that compartment. Conversely, a negative  $\Delta\Psi$  indicates a decrease of the expression of the distal ALE in that compartment. O) Frequency of Mbnl sequences (UGCU, CGCU, UGCC) throughout the UTRs of Mbnl sensitive (blue) and Mbnl insensitive (red) distal ALEs defined in CAD cells. Mbnl insensitive ALEs had  $\Delta\Delta\Psi$  values between -0.01 and 0.01 while Mbnl sensitive ALEs had  $\Delta\Delta\Psi$  values at least 1 SD below the mean (below -0.07). UTRs were binned into 100 bins across their length and the fraction of 4mers that matched a Mbnl kmer in each bin was recorded. Lines represent LOESS fits of values across the UTR while shaded areas represent 95% confidence intervals of the fit. P) Same as (O), but using Mbnl sensitive and insensitive ALE events and data from primary cortical neurons. Mbnl insensitive ALEs had  $\Delta\Delta\Psi$  values between -0.02 and 0.02 in both *Mbnl1* and *Mbnl2* knockouts while Mbnl sensitive ALEs had  $\Delta\Delta\Psi$  values below -0.05 in both knockouts (1 SD below the mean). Q) Distribution of  $\Delta\Delta\Psi$  values following Mbnl depletion in CAD cells as a function of Mbnl kmer density in the UTRs of those ALEs. R) Same as (Q), but  $\Delta\Delta\Psi$  values were calculated for localized ALEs in *Mbnl1* KO mice compared to WT mice. S) Same as (Q), but  $\Delta\Delta\Psi$  values are calculated for localized ALEs in *Mbnl2* KO mice compared to WT mice. T-V) Distribution of changes in localization (as  $\Delta\Delta\Psi$ ) as a function of Mbnl kmer density in UTRs of distal ALEs following *Mbnl1/2* knockdown in CAD cells (T), in primary cortical neurons of *Mbnl1*<sup>-/-</sup> mice (U), and in primary cortical neurons of *Mbnl2*<sup>-/-</sup> mice (V).  $\Delta\Delta\Psi$  is calculated as the  $\Delta\Psi$  in the Mbnl knockdown/knockout sample minus  $\Delta\Psi$  in the control/WT sample. Thus, a negative value represents a decrease in neurite localization for the distal ALE. Gray lines behind the boxes represent the median delta  $\Delta\Psi$  value for each kmer density for the top 3 preferred kmers of 20 RNA binding proteins.

### Supplementary Table Legends

**Supplementary Table 1. Related to Figure 1.** Correlations of localization ratios (LR) and  $\Delta\Psi$  values between different biological samples.

**Supplementary Table 2. Related to Figure 3.** Distal ALE isoforms associated with localization in neuronal cell lines. These distal ALEs come from ALE events with Bayes factors of at least 10 and delta PSI values of at least 0.1 in both N2A and CAD cell lines.

**Supplementary Table 3. Related to Figure 4.** Localization ratios following *Mbnl1/2* depletion in CAD cells. The listed genes had localization ratio changes at least one standard deviation below the mean. Membership in three gene ontology categories of neurological importance (GO:0016192, GO:0055085, and GO:0050877, respectively) is indicated by yes or no.

## **Supplementary Experimental Procedures**

### *Primary neuron culture and fractionation*

Cortices from E18.5 mice were dissected into 1 mL cold dissection buffer (1X HBSS). Cells were then trypsinized by adding trypsin to 0.25% and incubating for 20 min at 37° C. Trypsin was then inactivated by the addition of DMEM/FBS and the cortices were washed twice with DMEM/FBS. Cells were then resuspended in neurobasal media +50 µL / mL DNase and dissociated by gentle pipetting. The dissociated cells were then filtered through a 40 µm grid to eliminate chunks and counted. Approximately 3 million cells per membrane were plated on poly-D-lysine coated polyethylene terephthalate membranes with 1 µm pores (Millipore PIRP30R48). The cells were then cultured at 37° C for 48 h before fractionation. Because of the small RNA yield from the projections of these primary cells, RNA from 3 animals was combined for a single prep. The cell fractionation and RNA isolation was performed as described above. Each genotype tested was analyzed in duplicate. Mbnl1/Mbnl2 double knockout mice were generated as Mbnl1<sup>-/-</sup>;Mbnl2<sup>c/c</sup>;Nestin-Cre mice. These mice were Mbnl1 constitutive nulls and had Mbnl2 expression specifically ablated in the nervous system (Goodwin et al., 2015)

### *RNA-seq analysis*

The reads were mapped to the mm9 genome using Tophat2 (Kim et al., 2013) and the following options: -r 25 --coverage-search -G --library-type fr-firststrand. Transcript expression levels were quantified using cufflinks (Trapnell et al., 2010) and the following options: -g -b -u -N --library-type fr-firststrand. The replicates were then combined and alternative splicing differences between the fractions was analyzed using MISO (Katz et al., 2010). For comparison, we compared ALE PSI values produced by MISO to those calculated from quantifications using Salmon (Patro et al., 2015). These two values were highly concordant ( $R_{Spearman} = 0.7$ ).

For the sequencing of CAD cells before and after differentiation, CAD cells were plated in a 6 well plate. The media was then replaced with serum-containing (undifferentiated

cells) or serum-free (differentiated) media. The cells were then incubated at 37° C for 24 h, and RNA was collected using a Qiagen RNeasy Mini kit. Strand-specific libraries were made, and the pre- and post-differentiation samples were sequenced on an Illumina HiSeq sequencer in duplicate, yielding approximately 50 million read pairs per replicate. Reads were aligned, expression levels were quantified, and alternative splicing was analyzed as described above. Gene ontology enrichments and soma- and neurite-enriched genes were done using DAVID (Huang et al., 2009).

For primary neuron fractionation, non-strand-specific libraries were constructed using the Clontech Low Input Library Prep Kit (Clontech 634947) and Nugen Ovation RNAseq system v2 (Nugen 7102) for the Mbni single knockouts and double knockouts, respectively. These libraries were sequenced on an Illumina NextSeq sequencer with paired-end 75 base reads, yielding approximately 50-75 million read pairs per replicate. The reads were then aligned to the mm9 genome using STAR (Dobin et al., 2013) and the following options: --alignIntronMax 1000000 --outSAMstrandField intronMotif. Expression levels were quantified and alternative splicing was analyzed as described above.

#### *RNA FISH*

Stellaris probes were ordered from Biosearch Technologies against common regions of a reporter construct. The probes were labeled with CAL fluor red 635.

Approximately 25,000 CAD cells were plated onto poly-L lysine-coated coverslips in a 12 well plate. The cells were allowed to attach to the coverslip for one hour, after which the media was replaced with media lacking serum, and the cells were allowed to differentiate for 24 h. The next day, the media was replaced again with serum-free media, and the cells were then transfected with 1 µg plasmid containing the reporter construct using Lipofectamine LTX (Invitrogen 15338030). The cells were allowed to express the reporter construct for 48 h. Afterwards, the media was removed and the

coverslip rinsed with PBS. Cells were fixed in 3.7% formaldehyde for 10 min, permeabilized with 70% ethanol at 4° C for 1 h, and washed with wash buffer (10% formamide in 2X SSC). Probes were then hybridized in hybridization buffer (100 µg / mL dextran sulfate, 10% formamide, 2X SSC) at 37° C overnight. Coverslips were then washed with was buffer, and incubated with DAPI buffer (5 ng/µL DAPI in wash buffer) at 37° C for 30 min. Coverslips were then washed and mounted on slides using Fluoromount G.

Samples were imaged on an Applied Precision DeltaVision Microscope at 60X magnification, at wavelengths of 435 nm (DAPI), 632 nm (RFP), and 676 nm (CAL fluor red). Images were then quantified using ImageJ. Briefly, mean intensities in projections from 632 nm and 676 nm were calculated by dividing the total intensities for each wavelength by the area of the projection. RNA levels in the projection were then normalized to the RFP signal by dividing the 676 nm mean intensity by the 632 nm mean intensity.

#### *Analysis of localized isoforms by qPCR*

Six million CAD cells were transfected with 1.5 ug each of two constructs. One construct contained the distal UTR of the indicated gene attached to a reporter while the other contained the proximal UTR attached to a reporter. The cells were incubated for 8 hrs and then plated on porous membranes and serum was withdrawn. The cells were then incubated for 36 hrs and fractionated into soma and neurite fractions. RNA was collected from both fractions and reverse transcribed. qPCR was performed using oligos that amplified either the reporter-distal UTR fusion or the reporter-proximal UTR fusion. In total, six replicates were performed. In figure 2C, the neurite/soma ratios of the reporter-proximal UTR fusion for each gene were set to 1.

#### *RNA structure calculations*

Localized distal 3' UTRs were defined as UTRs from ALE events that had delta PSI values greater than or equal to 0.1 in both N2A and CAD samples. Soma proximal UTRs were defined as the 3' UTRs from the proximal ALE in these same events. Similarly, for ALE events not associated with localization, UTRs from the distal and proximal ALEs yielded the “nonlocalized distal” and “nonlocalized proximal” sets.

Regions homologous to UTRs of each class were identified in rat, human, dog, and cow using UCSC liftover tool. These sequences were then aligned using ClustalW (Larkin et al., 2007), and the resulting alignments were folded 100 nt at a time using RNAalifold (Bernhart et al., 2008), with the 100 nt window sliding 25 nt at a time. The median MFE for each UTR was then used for comparisons between classes of UTRs.

#### *kmer enrichment*

To define *kmers* enriched between distal and proximal UTRs in ALE events associated with localization, the number of occurrences of each *kmer* in the UTR classes was counted, and significantly enriched *kmers* were identified using Fisher's exact test. The resulting p values were then corrected using the Benjamini-Hochberg procedure.

#### *Conservation analysis*

To define conservation values across UTRs, each nucleotide was binned into one of 100 bins along the UTR length, and the average phastCons score from a 30-way alignment was calculated in each bin.

To define the conservation of individual *kmers* within the localized distal UTRs, each *kmer* at each position was defined as conserved if the sequence of the homologous position in the human genome was exactly conserved. Each *kmer* was thus conserved some fraction of the time. This fraction was compared to the conservation fraction of 50 control *kmers* with matched GC and CpG content to define a Z-score for each *kmer*.

### *CLIP data*

CLIP clusters were derived from previously published CLIP data sets (Wang et al., 2012; 2010; Yeo et al., 2009). The number of clusters present in each UTR was normalized by the length of the UTR to calculate a density. Densities were then compared between distal and proximal UTRs for events both associated and not associated with localization.

### *RNA decay experiments*

N2A cells were plated on porous membranes as described above. The cells were treated with 10 µg/mL actinomycin D (Sigma A1410) for the indicated times and then fractionated as described above. qRT-PCR was performed on RNA harvested from both cell body and projection fractions. qRT-PCR targets were chosen based on their observed level of enrichment in either soma or projection fractions. The 16S rRNA transcript was used as a control for normalization amongst the decay time points.

### *Analysis of NPC differentiation data*

RNA-seq data of a differentiation time course of human NPC into neurons was downloaded from GEO (GSE56785). For each time point, the replicates were combined, and the reads were mapped to hg19 using Tophat and default options. PSI values were then calculated for each junction using MISO.

### *Knockdown/fractionation*

For *Mbnl* knockdown experiments, approximately 150,000 CAD cells were plated in each well of a 6 well plate. Each well was then transfected with 100 pmol each of siRNA against *Mbnl1* and *Mbnl2* (Dharmacon) or 200 pmol of control siRNA

(Dharmacon) using Lipofectamine RNAiMAX (Invitrogen 13778030). Cells were then trypsinized and collected 48 h after transfection and replated on porous membranes as described above. The cells were differentiated using serum-free media for 24 h, then fractionated and harvested as described above. qRT-PCR was performed to confirm Mbnl knockdown, and soma and projection fractions from control and Mbnl knockdowns were each sequenced in triplicate.

*Binning ALEs based on  $\Delta\Delta\Psi$  value in Mbnl1/2 double knockouts*

Mbnl1/2 double knockouts were generated as constitutive Mbnl1 knockouts (Mbnl1 -/-) and conditional Mbnl2 knockouts in Nestin positive cells. ALEs were sorted by their  $\Delta\Delta\Psi$  values ( $\Delta\Psi$  in double knockout minus  $\Delta\Psi$  in wildtype). Thus, negative  $\Delta\Delta\Psi$  values represent a decrease in localization of the distal ALE isoform in the double knockout. Four categories of ALEs were defined. “Unchanged” ALEs had  $\Delta\Delta\Psi$  values between 0.01 and -0.01. “Slightly less localized” ALEs had values between 0 and 1 standard deviation below the mean. “Moderately less localized” ALEs had values between 1 and 2 standard deviations below the mean, and “strongly less localized” ALEs had values greater than 2 standard deviations below the mean.

*Analysis of the effects of cancer and development on ALEs and tandem UTRs*

Matched tumor and control RNA-seq datasets were downloaded for hepatocarcinomas (GSE25599) (Huang et al., 2011) and lung cancer (ERP001058) (Seo et al., 2012). Mouse ventricle development (GSE49906) (Giudice et al., 2014), cardiac differentiation of ES cells (GSE58363) (Devine et al., 2014), human NPC differentiation (GSE56785) (Sauvageau et al., 2013), and human fibroblast reprogramming (GSE60996) (Romero et al., 2015) datasets were also downloaded. These reads were mapped with STAR (Dobin et al., 2013) and the following options: --alignIntronMax 1000000 --outSAMstrandField intronMotif. Alternative splicing was analyzed as described above using MISO. For each sample, the fraction of significantly changing alternative splicing events that displayed increases in inclusion isoform expression and exclusion isoform expression were calculated.

## Supplemental References

- Bassell, G.J., Zhang, H., Byrd, A.L., Femino, A.M., Singer, R.H., Taneja, K.L., Lifshitz, L.M., Herman, I.M., and Kosik, K.S. (1998). Sorting of beta-actin mRNA and protein to neurites and growth cones in culture. *J Neurosci* *18*, 251–265.
- Bernhart, S.H., Hofacker, I.L., Will, S., Gruber, A.R., and Stadler, P.F. (2008). RNAalifold: improved consensus structure prediction for RNA alignments. *BMC Bioinformatics* *9*, 474.
- Devine, W.P., Wythe, J.D., George, M., Koshiba-Takeuchi, K., and Bruneau, B.G. (2014). Early patterning and specification of cardiac progenitors in gastrulating mesoderm. *eLife* *3*.
- Dobin, A., Davis, C.A., Schlesinger, F., Drenkow, J., Zaleski, C., Jha, S., Batut, P., Chaisson, M., and Gingeras, T.R. (2013). STAR: ultrafast universal RNA-seq aligner. *Bioinformatics* *29*, 15–21.
- Gao, Y., Tatavarty, V., Korza, G., Levin, M.K., and Carson, J.H. (2008). Multiplexed dendritic targeting of alpha calcium calmodulin-dependent protein kinase II, neurogranin, and activity-regulated cytoskeleton-associated protein RNAs by the A2 pathway. *Mol Biol Cell* *19*, 2311–2327.
- Giudice, J., Xia, Z., Wang, E.T., Scavuzzo, M.A., Ward, A.J., Kalsotra, A., Wang, W., Wehrens, X.H.T., Burge, C.B., Li, W., et al. (2014). Alternative splicing regulates vesicular trafficking genes in cardiomyocytes during postnatal heart development. *Nat Commun* *5*, 3603.
- Goodwin, M., Mohan, A., Batra, R., Lee, K.-Y., Charizanis, K., Gómez, F.J.F., Eddarkaoui, S., Sergeant, N., Buée, L., Kimura, T., et al. (2015). MBNL Sequestration by Toxic RNAs and RNA Misprocessing in the Myotonic Dystrophy Brain. *Cell Reports* *12*, 1159–1168.
- Huang, D.W., Sherman, B.T., and Lempicki, R.A. (2009). Bioinformatics enrichment tools: paths toward the comprehensive functional analysis of large gene lists. *Nucleic Acids Res* *37*, 1–13.
- Huang, Q., Lin, B., Liu, H., Ma, X., Mo, F., Yu, W., Li, L., Li, H., Tian, T., Wu, D., et al. (2011). RNA-Seq analyses generate comprehensive transcriptomic landscape and reveal complex transcript patterns in hepatocellular carcinoma. *PLoS ONE* *6*, e26168.
- Katz, Y., Wang, E.T., Airoldi, E.M., and Burge, C.B. (2010). Analysis and design of RNA sequencing experiments for identifying isoform regulation. *Nat Methods* *7*, 1009–1015.
- Kim, D., Pertea, G., Trapnell, C., Pimentel, H., Kelley, R., and Salzberg, S.L. (2013). TopHat2: accurate alignment of transcriptomes in the presence of insertions, deletions

and gene fusions. *Genome Biol* 14, R36.

Larkin, M.A., Blackshields, G., Brown, N.P., Chenna, R., McGettigan, P.A., McWilliam, H., Valentin, F., Wallace, I.M., Wilm, A., Lopez, R., et al. (2007). Clustal W and Clustal X version 2.0. ....

Patro, R., Duggal, G., and Kingsford, C. (2015). Salmon: Accurate, Versatile and Ultrafast Quantification from RNA-seq Data using Lightweight-Alignment | bioRxiv. bioRxiv.

Romero, I.G., Pavlovic, B.J., Hernando-Herraez, I., Zhou, X., Ward, M.C., Banovich, N.E., Kagan, C.L., Burnett, J.E., Huang, C.H., Mitrano, A., et al. (2015). A panel of induced pluripotent stem cells from chimpanzees: a resource for comparative functional genomics. *eLife* 4, e07103.

Sauvageau, M., Goff, L.A., Lodato, S., Bonev, B., Groff, A.F., Gerhardinger, C., Sanchez-Gomez, D.B., Hacisuleyman, E., Li, E., Spence, M., et al. (2013). Multiple knockout mouse models reveal lincRNAs are required for life and brain development. *eLife* 2, e01749.

Seo, J.-S., Ju, Y.S., Lee, W.-C., Shin, J.-Y., Lee, J.K., Bleazard, T., Lee, J., Jung, Y.J., Kim, J.-O., Shin, J.-Y., et al. (2012). The transcriptional landscape and mutational profile of lung adenocarcinoma. *Genome Res* 22, 2109–2119.

Trapnell, C., Williams, B.A., Pertea, G., Mortazavi, A., Kwan, G., van Baren, M.J., Salzberg, S.L., Wold, B.J., and Pachter, L. (2010). Transcript assembly and quantification by RNA-Seq reveals unannotated transcripts and isoform switching during cell differentiation. *Nat Biotechnol* 28, 511–515.

Wang, E.T., Cody, N.A.L., Jog, S., Biancolella, M., Wang, T.T., Treacy, D.J., Luo, S., Schroth, G.P., Housman, D.E., Reddy, S., et al. (2012). Transcriptome-wide Regulation of Pre-mRNA Splicing and mRNA Localization by Muscleblind Proteins. *Cell* 150, 710–724.

Wang, Z., Kayikci, M., Briese, M., Zarnack, K., Luscombe, N.M., Rot, G., Zupan, B., Curk, T., and Ule, J. (2010). iCLIP predicts the dual splicing effects of TIA-RNA interactions. *PLoS Biol* 8, e1000530.

Yeo, G.W., Coufal, N.G., Liang, T.Y., Peng, G.E., Fu, X.-D., and Gage, F.H. (2009). An RNA code for the FOX2 splicing regulator revealed by mapping RNA-protein interactions in stem cells. *Nat Struct Mol Biol* 16, 130–137.

Yudin, D., Hanz, S., Yoo, S., Iavnilovitch, E., Willis, D., Gradus, T., Vuppalanchi, D., Segal-Ruder, Y., Ben-Yaakov, K., Hieda, M., et al. (2008). Localized regulation of axonal RanGTPase controls retrograde injury signaling in peripheral nerve. *Neuron* 59, 241–252.